Magazine of Civil Engineering. 2019. 92(8). Pp. 36–47
Инженерно-строительный журнал. 2019. № 8(92). С. 36–47

Magazine of Civil Engineering

ISSN 2071–0305

journal homepage: http://engstroy.spbstu.ru/

DOI: 10.18720/MCE.92.3

Strength and microstructure of alkali-activated natural pozzolan and limestone powder mortar

A.A. Adewumi[a], M. Ismail[a]*, M.A.M. Ariffin[a], M.O. Yusuf[b], M. Maslehuddin[c], H.D. Mohamed[c]
[a] Universiti Teknologi Malaysia, Johor Bahru, Malaysia
[b] Univeristy of Hafr Albatin, Hafr Al-Batin, Saudi Arabia
[c] King Fahd University of Petroleum and Minerals, Dhahran, Saudi Arabia
** E–mail: mohammad@utm.my*

Keywords: alkali-activated mortar, natural pozzolan, limestone powder, microstructure, aluminosilicate, compressive strength

Abstract. In this study, the synergistic effects of natural pozzolan (NP) and limestone powder waste (LSPW) alkaline activated mortar has been investigated using compressive strength and microstructure analysis. LSPW was added in varying percentages to alkaline activated NP such that the combined ratio (LSPW/(LSPW + NP)) varied from (0 to 1) at the interval of 0.2. The activators used were sodium silicate ($Na_2SiO_{3(aq)}$) and sodium hydroxide (10M $NaOH_{(aq)}$) combined as 1:1. The findings revealed that the synergistic effect of NP with LSPW emanated from silica and alumina required for the formation of aluminosilicate framework which required cation sourced from LSPW (Ca^{2+}) for charge balancing in the formed skeletal framework. The products formed were mainly anorthite ($CaAl_2Si_2O_8$) and gehlenite ($CaO.Al_2O_3.SiO_2$). Besides, about 77 % of 28-days compressive strength (27 MPa) could be achieved in 24 h using heat curing. Microstructural analysis revealed that the rough texture of activated NP characterized with high porosity turned to be filled up by the presence of LSPW thereby improving the microstructural density.

1. Introduction

Ordinary Portland cement (OPC), the main hydraulic binder in concrete is the largest manufactured binder globally [1]. OPC world production was estimated to be 4.6 billion tonnes in the year 2015 with a projection of four-fold increase by 2050 [2]. One of the negative sides of OPC is its contribution of CO_2 to the environment and the fuel consumption during its manufacturing process. OPC calcination process significantly leads to the emission of 5–8 % of global CO_2 into the atmosphere which has greatly contributed to the depletion of the ozone layer [3, 4]. Climate change is mainly due to greenhouse gas (GHG) emissions, of which CO_2 is a major contributor, it accounts for 82 % of the total GHG [3].

Alkali-activated material (AAM) has been identified as an eco-efficient and economically viable alternative for replacing OPC due to its excellent strength, thermal and low permeability [5, 6]. AAM is a system formed by the reaction of soluble alkali activator and aluminosilicate precursors [5]. AAM is classified into low calcium (fly ash, metakaolin and natural pozzolans) and high calcium (blast furnace slag) binders. The main products in low binder AAM could be mainly potassium/sodium aluminosilicate hydrate with impregnation of alumina (NASH and KASH) within the formation. In high calcium binder such as blast furnace slag that is synthesized with a mild alkali, the main product is calcium alumina silicate hydrate [7].

Many researchers have successfully synthesized alkali-activated mortars and concretes from volcanic materials such as natural pozzolan (NP) [7–9], agricultural waste materials such as, rice husk ash [10], palm oil fuel ash (POFA) [10–14] or industrial waste such as silico-manganese slag (SiMn) [15], ground granulated blast furnace

Adewumi, A.A., Ismail, M., Ariffin, M.A.M., Yusuf, M.O., Maslehuddin, M., Mohamed, H.D. Strength and microstructure of alkali-activated natural pozzolan and limestone powder mortar. Magazine of Civil Engineering. 2019. 92(8). Pp. 36–47. DOI: 10.18720/MCE.92.3

Адевуми А.А., Исмаил М., Ариффин М.А.М., Юсуф М.О., Маслехуддин М., Мохамед Х.Д. Прочность и микроструктура щелочно-активированного пуццоланового и известнякового раствора // Инженерно-строительный журнал. 2019. № 8(92). С. 36–47. DOI: 10.18720/MCE.92.3

slag (GGBFS) [15–17], fly ash (FA) [18], silica fume (SF) [18, 19], coal bottom ash [20], paper sludge ash [21] and mine tails [5] with aluminosilicate components. Fly ash (class F), silica fume, and slag have been shown to be a good precursor for alkali-activated concrete, however, the proliferation of environmental wastes and the need to improve public health have called for utilization of other solid wastes for alkali-activated binders.

This research has identified natural pozzolan (NP) and limestone powder wastes (LSPW) in the synthesis of alkali-activated binder. NP is formed from a volcanic eruption with very high silica and moderate alumina contents. The world reserve of NP has been estimated to be 7 billion tons [22] while 180,000 km^2 of NP is also available in the western region of Saudi-Arabia [23]. Furthermore, significant deposits of NP have been reported in China, Turkey, Greece, Iran and the USA [24]. Due to NP chemical compositions and its plethora availability across the volcanic regions, it has gained global acceptance for the synthesis of geopolymer concrete [25]. The production of limestone tiles by diamond cutting of limestone rock generates millions of tonnage of limestone powder wastes (LSPW). Limestone quarry generates around 20 % to 25 % powder waste [26]. About 21.2 million tons of LSPW is generated in the UK, while in Greece, 18 million tons are generated and Turkey generates 30 million tons per annum [26]. LSPW are deposited in landfills, the dust particles from the landfills contaminate the air as a result of wind blow, these have resulted in environmental, air and water pollution leading to severe health hazards such as cancer and asthma [27]. LSPW has been used as filler in concrete to enhance the compressive strength of concrete [27, 28].

In some of the previous studies on NP, Ghafoori et al. [29] studied the effect of alkali activators parameter on alkali-activated NP mortar. However, the influence of alkaline-activator on microstructure of the resulted products was not explored. In another study, Ibrahim et al. [30] studied similar effects under continuous heat curing condition at 60 °C for 28 days. Furthermore, the binary effect of blast furnace slag (BFS) and NP on the strength development of mortars cured at room temperature has been investigated and it was found that the CaO in slag contributed to the improved strength as a result of the formation of Ca-Al-Si gel in the matrix [7]. Silva et al. [25] synthesized geopolymer concrete using fired clay brick waste and NP, also under continuous oven curing for 7days. Oven curing for long days will result in high consumption of energy. Cwirzen et al. [31] investigated the blends of metakaolin and limestone alkali-activated paste using NaOH only, which show relatively low strength of 7MPa. Yuan et al. [32] found that 30 % of limestone powder could improve the strength of sodium carbonate activated slag.

Several environmental friendly waste materials have been studied by researchers, however, despite these numerous works on the performance of alkali-activated binders, none of these studies has addressed the engineering properties of activated mortar using a blend of limestone powder and natural pozzolan. So far, the effects of LSPW on the reaction products, strength development, bond characteristics and the microstructure of LSPW/NP alkali-activated mortar are yet to be investigated. Therefore, the present research aims at studying the synergistic effect of LSPW/NP on the reaction products, strength development, bond characteristics and the microstructure of the product matrix. The outcomes of this study will contribute to waste valorization, dumpsite land reclamation, low CO_2 footprint, energy consumption reduction, reduction in environmental pollution and addition to more sustainable alternative binders for structural purposes.

2. Materials and Methods

2.1. Materials and reagents

2.1.1. Natural pozzolan and limestone powder waste

Natural pozzolan (NP) was provided by Imerys minerals Arabia and the limestone powder waste (LSPW) was obtained from tiles cutting factory. The LSPW was oven-dried at 105 °C ± 5 °C for 24 hrs to remove the moistures. The LSPW was sieved through sieve 200 μm sieve to remove stones and debris. The particle size distributions (PSDs) of precursors were determined with the aid of HELOS (H3533) & QUIXEL particle size analyzer using sedimentation method and X-ray absorption, while the specific surface areas (BET) of the precursors were determined with Micromeritics ASAP2020 by using nitrogen gas adsorption, the results are presented in Table 1 and Figure. 1. The oxide compositions of these two materials as revealed in Table 2 were determined by using X-ray fluorescence (XRF) machine.

The morphology of the powdered LSPW and NP was evaluated using a JSM-5800LV scanning electron microscope (SEM). As revealed in Figure. 2, LSPW has a round edge polycrystal-like shape, while NP has an angular particle shape coupled with elongated flakiness. The mineralogical composition and amorphous or crystalline nature of the raw materials were explored using X-ray diffraction (XRD) analysis. The crystalline phases were identified from the COD database (2019 edition) in conjunction with the MATCH XRD software. According to the XRD result shown in Figure. 3, NP contains mainly quartz (SiO_2), plagioclase (Ca, Na)$Al_2Si_2O_8$) and microcline ($KAl_2Si_2O_8$), it revealed that NP is an amorphous compound with very low crystallinity while the LSPW contains mainly calcite ($CaCO_3$) and quartz ((SiO_2) and it is of high crystallinity.

Table 1. Physical properties of NP and LSPW.

Materials	Specific gravity	Average particle size, d_{50} (µm)	Specific surface area (cm^2/g)
NP	2.3	4.84	3.1
LSWP	2.7	6.43	0.6

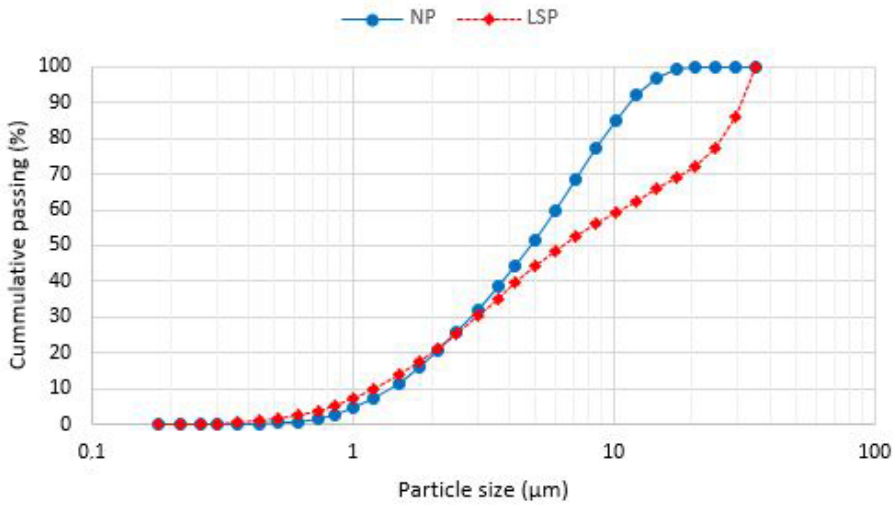

Figure 1. Particle size distribution of LSP and NP.

Table 2. Chemical compositions of NP and LSPW obtained from XRF.

Oxides	SiO_2	CaO	Al_2O_3	Fe_2O_3	MgO	Na_20	K_20	$S0_3$	L.O.I
LSPW (%)	2.5	94.1	0.8	1.2	0.6	-	0.3	0.5	44
NP(%)	74	2	13	1.5	0.5	4	5	-	5

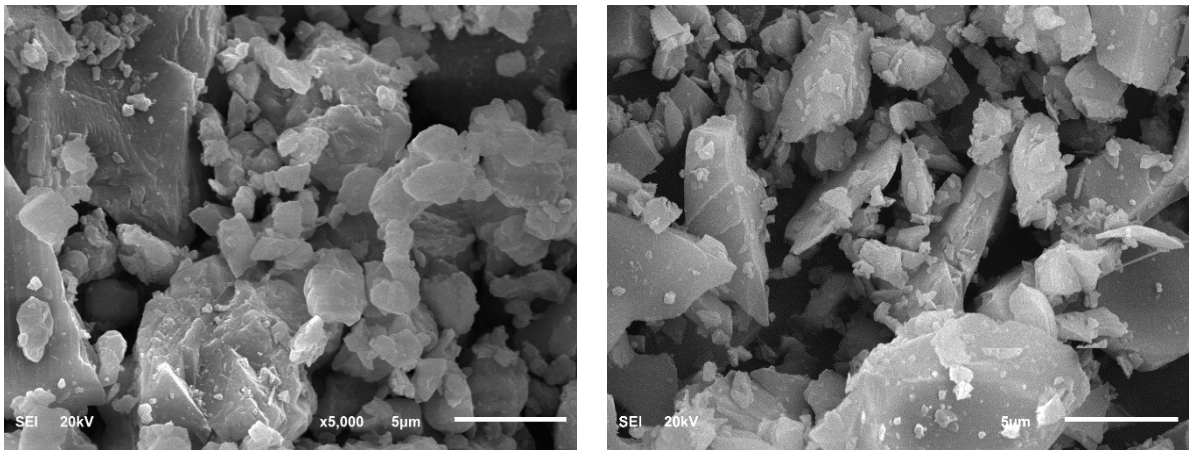

(a) (b)

Figure 2. SEM micrographs of raw materials: (a) LSPW and (b) NP.

2.1.2. Synthesis of alkali activator

Sodium silicate (SS) and sodium hydroxide (NH) that are commercially available were used as activators in this study. The initial silica modulus (Ms = SiO_2/Na_2O) was 3.3 while the molarity of $NaOH_{(aq)}$ (NH) was 10 M. The percentage composition of SS is as follows: H_2O: 62.11 %, SiO_2: 29.13 % and Na_2O: 8.76 %. The 10 M-$NaOH_{(aq)}$ was prepared by dissolving 404.4 g of NaOH pellet (99 % assays) into distilled water to form 1 L of an alkali solution (10 M-$NaOH_{(aq)}$).

2.1.3. Aggregates

Dune desert sand passing the gradation size requirement of ASTM C33 was used as fine aggregate (FA), The fineness modulus of FA was 1.82 and the specific gravity in saturated surface dry (SSD) condition was 2.63.

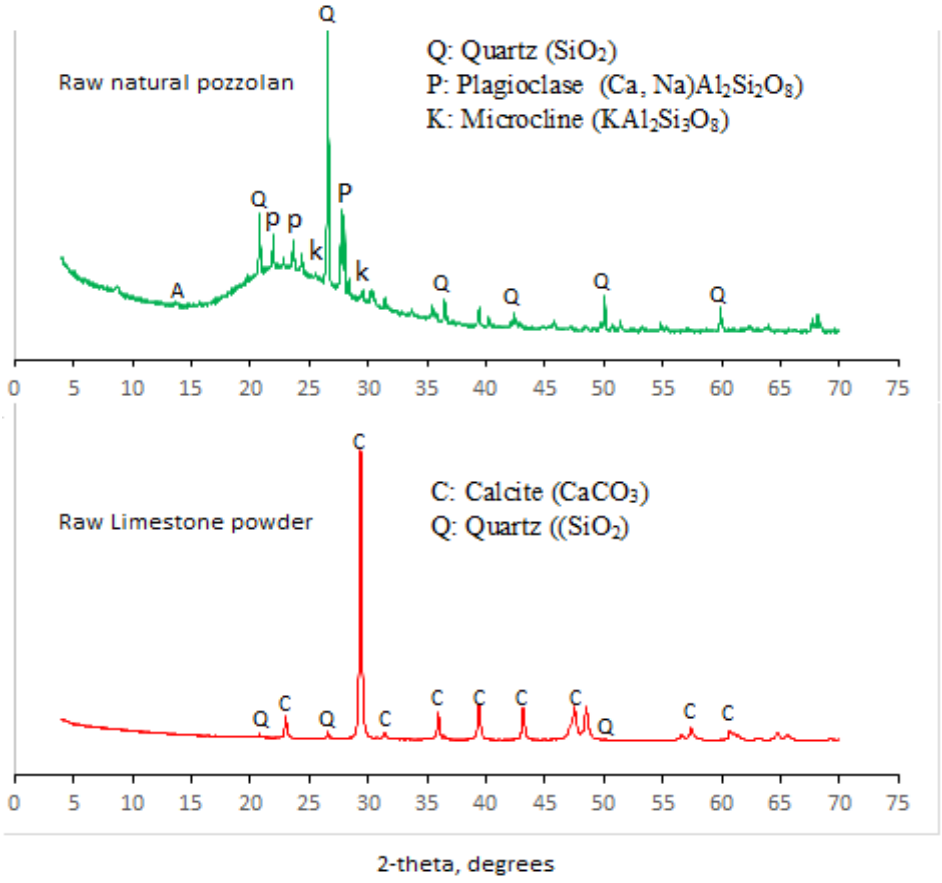

Figure 3. X-ray diffractograms: (a) Raw natural pozzolan and (b) Raw limestone powder.

2.2. Experimental program

2.2.1. Mix design

The mixture proportions of alkali-activated mortar were designed with LSPW content of 0 %, 20 %, 40 %, 60 % 80 % and 100 % (natural pozzolan contents of 100 %, 80 %, 60 %, 40 %, 20 % and 0 %, respectively). The samples were designated as $AANL_x$ (alkali-activated NP/LSPW mortar), where x is the $\frac{L}{L+N}$ ratios. A total of six $AANL_x$ (where x = 0, 0.2, 0.4, 0.6. 0.8 and 1) mixtures were prepared. $AANL_0$ and $AANL_1$ served as the control. Table 3 summarizes the proportion of the constituent materials in the alkali-activated mortar mixtures. A constant fine aggregate -to-the binder ratio of 2 was used. This was the optimum value from our preliminary trial mix. All the mixtures were prepared using Na_2SiO_3(aq)/ $NaOH_{aq}$ (NS/NH) ratio of 1.0 and alkali activator to binder ratio of 0.5 for the mortar and 0.25 for the paste. In all the mixtures, The free water to precursor ratio was maintained 10 %.

Table 3. Mixture proportion of alkali-activated natural pozzolan/limestone powder waste mortar.

Mix #	Mix ID.	NP kg/m^3	LSPW kg/m^3	$Na_2SiO_{3(aq)}$ (NS) kg/m^3	$NaOH_{(aq)}$ (NH) kg/m^3	Water kg/m^3	Sand kg/m^3
M1	$AANL_0$	605	0	151.5	151.5	60.5	1210
M2	$AANL_{0.2}$	484	121	151.5	151.5	60.5	1210
M3	$AANL_{0.4}$	363	242	151.5	151.5	60.5	1210
M4	$AANL_{0.6}$	242	363	151.5	151.5	60.5	1210
M5	$AANL_{0.8}$	121	484	151.5	151.5	60.5	1210
M6	$AANL_1$	0	605	151.5	151.5	60.5	1210

2.2.2. Sample preparation, mixing, placing and curing

The required quantities of constituent materials were measured and mixed in batches in 5.0 L capacity Hobart planetary bench mixer, the mixing of the materials was in two stages. First, the NP and LSPW powder and sand were mixed in a dry condition for 3 mins. Secondly, the alkali solution ($NaOH_{(aq)}$ +$Na_2SiO_{3(aq)}$) and water were added for the wet mixing stage which involves low speed mixing for 2mins and another 4 mins for

fast or higher speed mixing until a homogeneous mixture was achieved, the total mixing time was about 9 to 10 min. It should also be noted that 10M NaOH(aq) was prepared a day prior to mixing to allow cooling of the solution due to the exothermic nature of the solution. Thereafter, the mortar was placed in the oil-smeared steel moulds of 50×50×50 mm in two layers and each layer was vibrated on the vibrating table for 30 s to remove any entrapped air from the mixture. Follow by surface smoothening of the specimen with a hand trowel. The specimens were then covered with a plastic sheet to prevent moisture loss. Afterwards, the specimens were kept in the laboratory at 20 ± 5 °C for 24 hrs. The cubes were de-moulded after 24 hrs. This was followed by placing the samples in zip plastic bags to avoid loss of moisture to the environment. The samples were then subjected to temperature curing in an oven maintained at 75 °C for 24 hrs. After that, the specimens were cured under a normal condition of 20 ± 5 °C until the age of testing (1, 3, 7, 14 and 28 days). The mineralogical and morphological analysis in this study was conducted by using a paste of the alkali-activated material.

2.3. Evaluation methods

2.3.1. Setting time and workability

The initial and final setting times of the AANL paste were determined in accordance with ASTM C191 [33] and the workability of AANL mortar was measured in accordance with ASTM C1437 [34].

2.3.2. Compressive strength

Compressive strength of the AANL mortar was determined in accordance with ASTM C 150 [35] on cube specimens measuring 50×50×50 mm using a digital compression testing machine. The compressive strength of the specimens was determined after 1, 3, 7, 14 and 28 days of curing. Three specimens were tested at each age and the average compressive strength value is reported.

2.3.3. Microstructural characterization of the specimens

X-ray diffractometer (XRD), scanning electron microscopy coupled with energy dispersive X-ray spectroscopic analysis (SEM + EDS) and Fourier transform spectroscopy (FTIR) were used to characterize the microstructure of the products and to determine the contribution of LSPW to the nature of the alkali-activated product, $AANL_0$, $AANL_1$ were compared with $AANL_{0.6}$, $AANL_0$, and $AANL_1$ served as the control specimens. The bond vibrations of the fine powder product obtained from 25 mm cube of AAP specimen after 14 days of curing were observed by using a Perking Elmer 880 spectrometer FTIR machine. The morphological study of the middle portions of the 25 mm cube of AAP specimens was done with the aid of the JEOL SEM + EDS model 5800 LV at accelerating voltage of 20 kV. The phases of the product were explored using XRD Bruker instrument model d2-Phaser with Cu Ka radiation (40 kV, 40 mA) by continuous scanning within angle 2-theta range of 4–80° and at a scan speed of 2.5°/min.

3. Results and Discussion

3.1. Effect of LSPW on workability alkaline-activated NP

The slump flow of the fresh $AANL_x$ (x = LSPW/(LSPW + NP) varies from 0 to 1) mixture is presented in Figure 4. The flow of the $AANL_0$ is the lowest in the mix, this phenomenon can be due to higher water demand of NP caused by high silica content (74 %). NP also has an angular particle shape coupled with elongated flakiness [Figure 2b] and larger specific surface area [Table 1] compared to LSPW. However, upon addition of LSPW to the alkali-activated NP mortar, it leads to an increase in the flowability of the mixture. There were 40 %, 90 %, 105 %, 120 % and 125 % increment in $AANL_{0.2}$, $AANL_{0.4}$, $AANL_{0.6}$, $AANL_{0.8}$ and $AANL_1$, respectively, when compared with $AANL_0$. This observation is due to high dissolution rate of LSPW in alkali activator compared to NP. This resulted in the micro-filling effect of the finer particle of LSPW within the matrix. The micro-filling effect positively enhanced the early strength in the synergized AANL as shown in Figure 5. This is in agreement with previous studies that showed that finer particle size distribution could contribute to better flowability [36, 37]. Equation 1 shows the correlation between the experimental values.

$$y = -14.063x^2 + 26.634x + 9.939. \quad (1)$$

3.2. Effect of LSPW on setting time of alkaline-activated NP

As shown in Figure 6, the incorporation of LSPW to $AANL_x$ (x = LSPW/(LSPW+NP) varies from 0 to 1) mixture generally leads to a reduction in setting time of the mixtures. The $AANL_0$ with 100 % NP has very high initial and final setting time as shown in Figure 2, however, when 20 % of LSPW was added to the mix, its initial setting time and final setting time reduced by 41 % and 64 % respectively, Further addition of 20 % LSPW ($AANL_{0.4}$) to the mix leads to a reduction of 76 % and 79 % of the initial setting time and final setting time, respectively in reference to $AANL_0$. Similar trends were observed upon total addition of 60 %, 80 % and 100 % of LSPW to the mixture. It should be noted that with 100 % LSPW, false setting was observed due to high reactivity of LSPW in alkali activators. The model equations predicting the results for the initial and final setting time in terms of x (x = LSPW/(LSPW+NP) is shown in Figure 6.

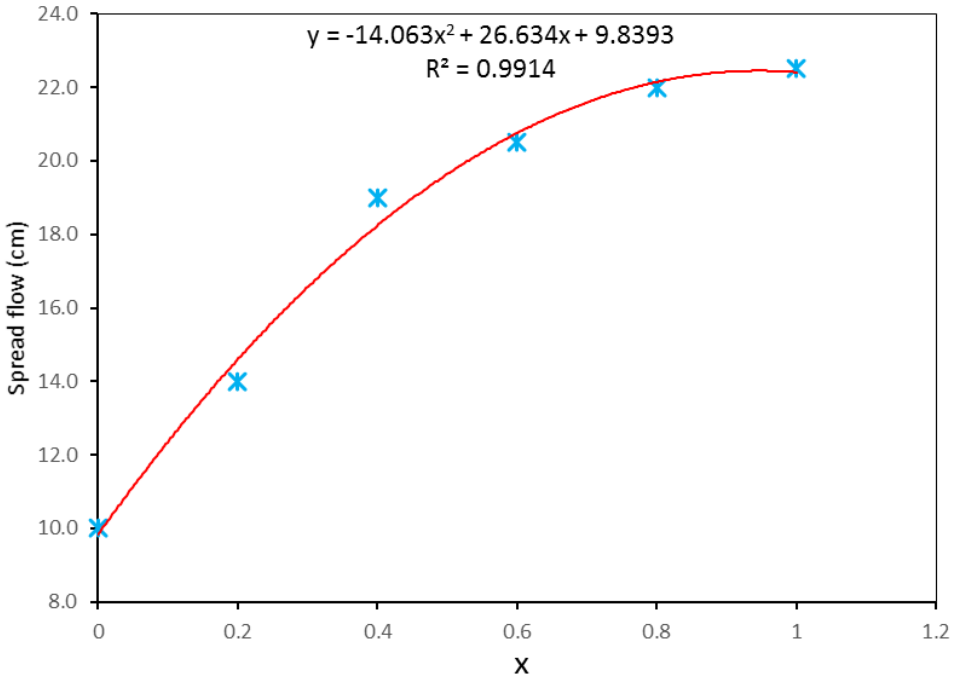

Figure 4. Flowability of the AANL.

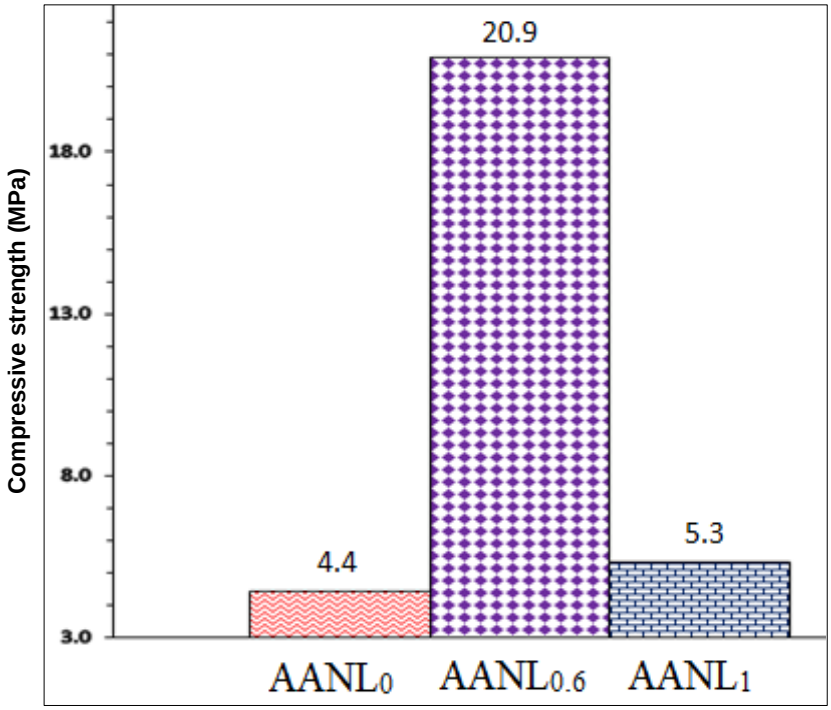

Figure 5. 1-day compressive strength of alkali-activated mortar.

3.3. Effect of LSPW on compressive strength of alkaline-activated NP

The synergistic effect of LSPW and NP on the compressive strength of synthesized alkali-activated mortar is shown in Figure 7. Generally, the compressive strength for all the mixes increases with age. The 1-day compressive strength of 4.4 MPa was obtained in $AANL_0$ which was 21.3 % of the strength obtained upon substituting NP with 20 % LSPW. The increase in strength continued as the substitution level increases as shown in Figure 7. The strength increased by 370.45 %, 322.7 %, 375 %, 193 % when 20 %, 40 %, 60 % and 80 % of LSPW were added to the mix proportion in $AANL_{0.2}$, $AANL_{0.4}$, $AANL_{0.6}$, $AANL_{0.8}$, respectively. The compressive strength of the mortar increase with LSPW content up to 60 % ($AANL_{0.2}$, $AANL_{0.4}$ and $AANL_{0.6}$) and then drastically decline upon 80 % LSPW ($AANL_{0.8}$) addition. While the 1-day compressive strength of 5.3 MPa was obtained in $AANL_1$. At 28days, 102.27 % of strength was gained in $AANL_0$. while 18.87 % was gained in $AANL_1$. The maximum strength of 27 MPa was obtained in $AANL_{0.6}$ after 28 days. It is remarkable that the combination of LSPW and NP in the synthesis of the AAM enhanced early strength development of the mixed than individual usage of the primary material.

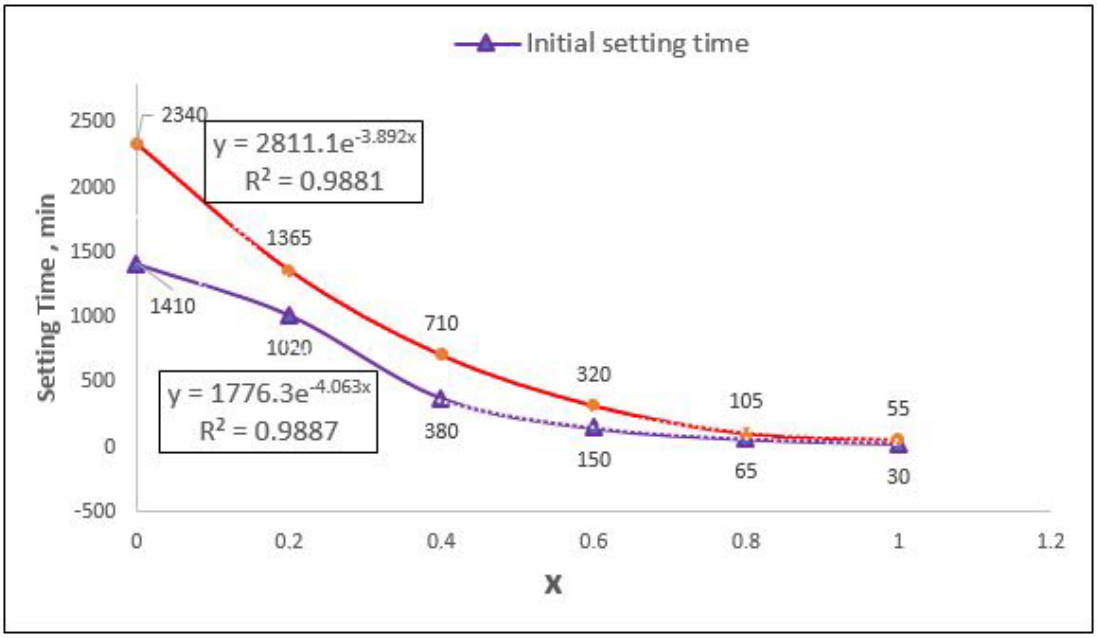

Figure 6. Setting time of AANL.

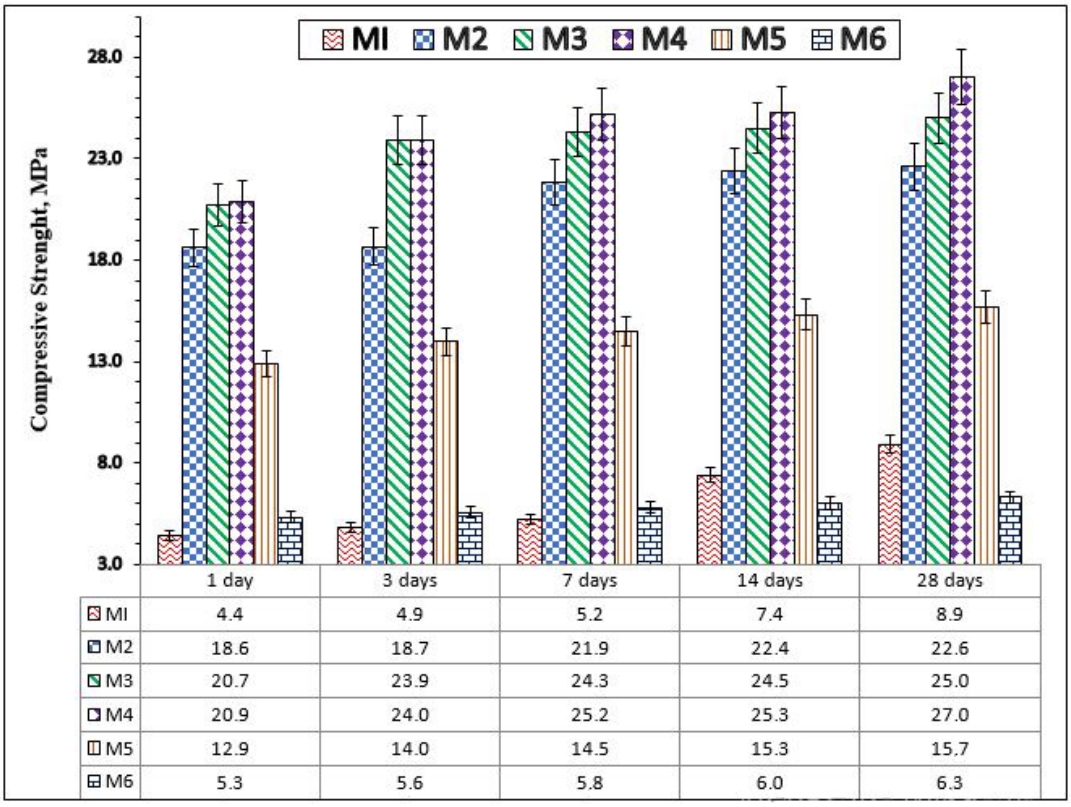

	1 day	3 days	7 days	14 days	28 days
MI	4.4	4.9	5.2	7.4	8.9
M2	18.6	18.7	21.9	22.4	22.6
M3	20.7	23.9	24.3	24.5	25.0
M4	20.9	24.0	25.2	25.3	27.0
M5	12.9	14.0	14.5	15.3	15.7
M6	5.3	5.6	5.8	6.0	6.3

Figure 7. Compressive strength of AANL mixes
(M1 = $AANL_0$, M2 = $AANL_{0.2}$, M3 = $AANL_{0.4}$, M4 = $AANL_{0.6}$, M5 = $AANL_{0.8}$, M6 = $AANL_1$)

3.4. Effect of limestone powder on microstructures and bonds of alkali-activated mortar

Limestone powder waste (LSPW) contains mainly CaO (94.1 %) and SiO_2 (2.5 %) with a little percentage of Al_2O_3 (0.8 %) as shown in Table 2, this can be expressed empirically as $Ca_{118}AS_3$. The XRD results in Figure 3 also confirmed the presence of high crystalline calcite ($CaCO_3$) and quartz (SiO_2). Alkali activation of LSPW starts by the breaking down of the LSPW bonds which mainly comprises calcite that breaks down into lime and carbon dioxide as shown in Equation 2 thereby making CaO available to play the charge balancing role in the stability of the oligomer formed from the condensation process of the transported silicate dominated monomers.

$$CaCO_3 \rightarrow CaO+CO_2. \quad (2)$$

Alkali activators most specifically, $NaOH_{(aq)}$ caused the dissolution of complex aluminosilicate, most especially during the early reactions thereby releasing the monomers such as Ca-O, Si-O-Si, Al-O-Al and

Al-O-Si together with that obtained from sodium silicate activators (Si-O-Si). $Na_2SiO_{3(aq)}$ and $NaOH_{(aq)}$ dissociate according to Equations 3 and 4

$$Na_2SiO_3(aq) \rightarrow Na_2O + SiO_2 + H_2O \quad (3)$$

$$NaOH_{(aq)} \rightarrow Na_2O + SiO_2 + H_2O \quad (4)$$

The SiO_2 from $Na_2SiO_{3(aq)}$ supplies the soluble Si ions while $NaOH_{(aq)}$ provides the OH^- for bond cleaving [38]. There is an exchange of H^+ for Ca^{2+} and Na^+ when the PH of the medium is between 7–10 during the early stage of the reaction, followed by the hydrolysis of Si-O-Si, Al-O-Al, or Al-O-Si to form Si-O-CaOH monomers [37]. The monomers polymerized to form $CaSiO_3$ (wollastonite), albite ($NaAlSi_3O_8$), and chains of SiO_2 as revealed in Figure 8b ($AANL_1$). The Ca^{2+} could also have reacted with OH^- to form portlandite ($Ca(OH)_2$), FTIR in Figure 9c confirms the precipitation of portlandite due to the increase in the intensity of OH^-, vibrating at wavenumber 3450 cm^{-1} which is not present in the raw LSPW as shown in Figure 8a. A very low 28-day compressive strength of 6.3 MPa was obtained in $AANL_1$, this was due to the formation portlandite ($Ca(OH)_2$) as explained previously.

In addition to this, FTIR in Figure 9c shows that there is an asymmetric stretching of H-O-H formed due to hydrogen bonding at a wavenumber of 2359 cm^{-1} coupled with bending of an unbound water molecule at 1645 cm^{-1}. Furthermore, Figure 10 shows the SEM image and the EDS result of $AANL_1$ which has an interconnected porous microstructure, that is responsible for the low compressive strength recorded. The EDS results also show very low content of Si (0.8 %) and Al (0.2 %) in spectrum 1 alongside with Si (1.4 %) and Al (0.2 %) in spectrum 3. Spectrum 2 reveals the presence of CaO in the matrix which can mix with entrapped water in the matrix as earlier stated to form ($Ca(OH)_2$). All these could contribute to the negative strength development in the $AANL_1$

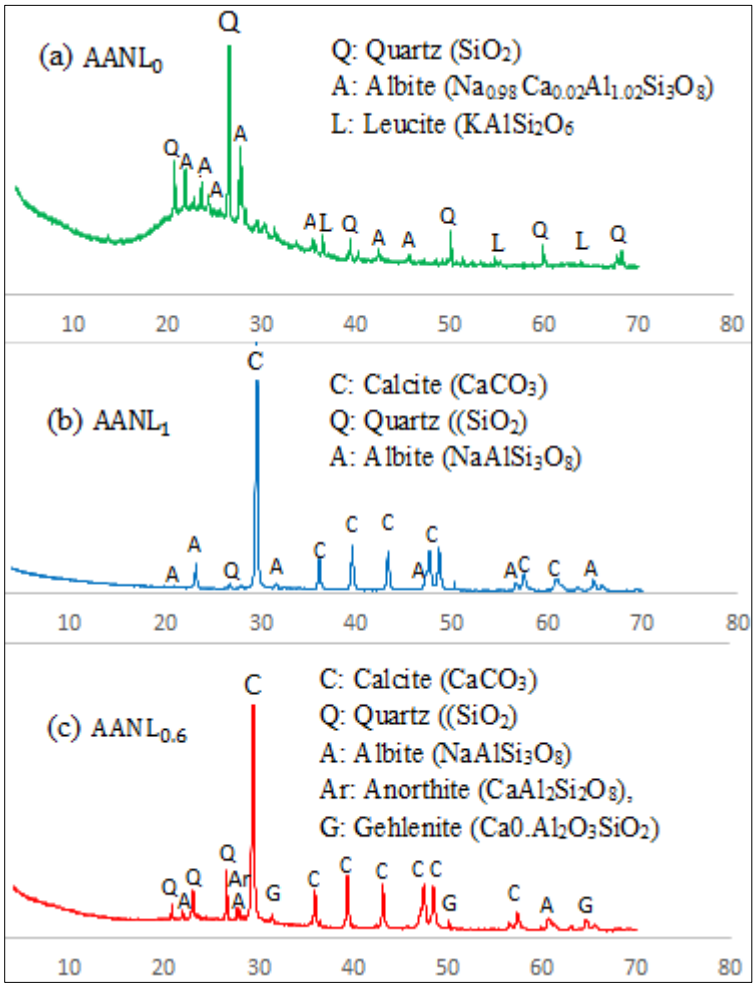

Figure 8. X-ray diffractograms of the activated product of (a) NP (b) LSPW (c) combined NP and LSPW.

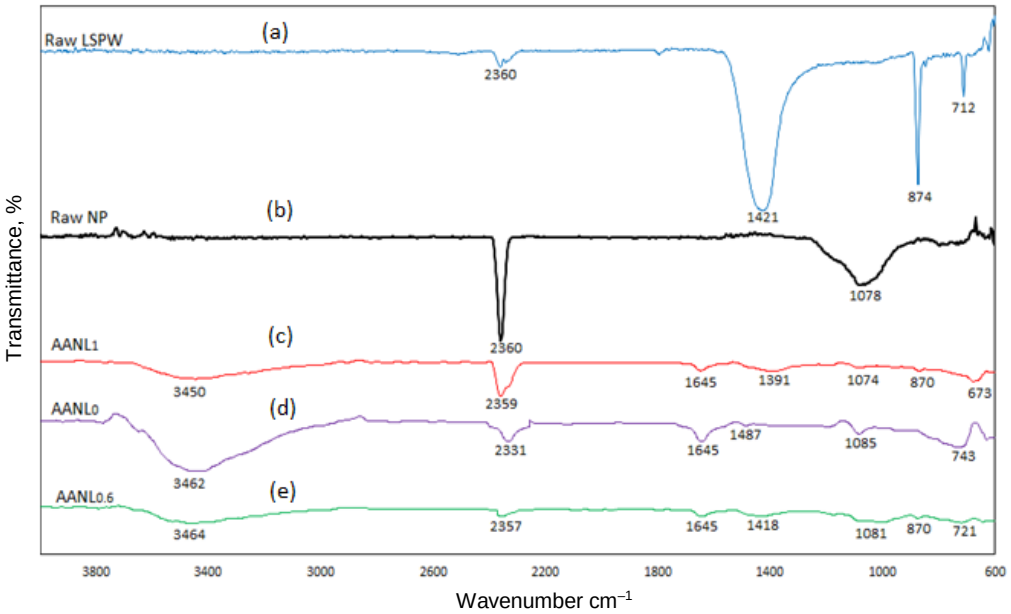

Figure 9. FTIR spectra of (a) unactivated limestone powder (b) unactivated natural pozzolan (c) activated limestone powder waste (d) activated natural pozzolan (e) activated limestone powder wastes and natural pozzolan.

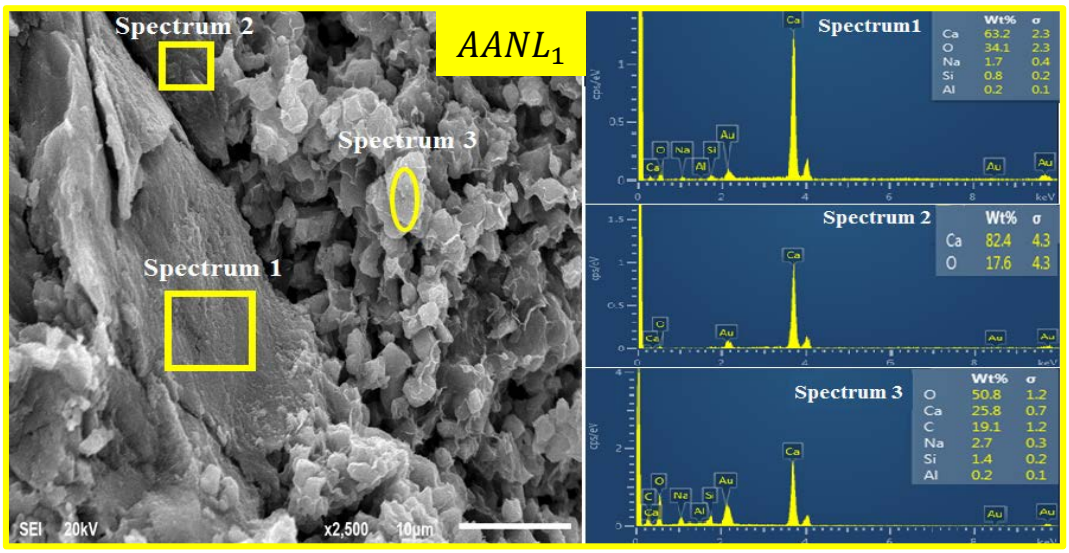

Figure 10. SEM/EDS of alkali-activated limestone powder wastes ($AANL_1$).

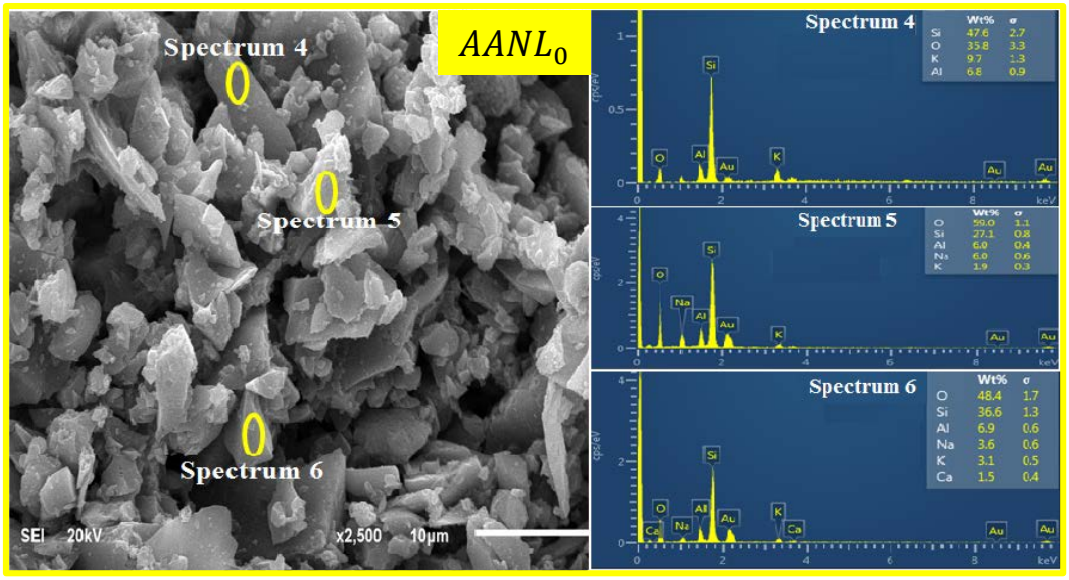

Figure 11. SEM/EDS of alkali-activated natural pozzolan ($AANL_1$).

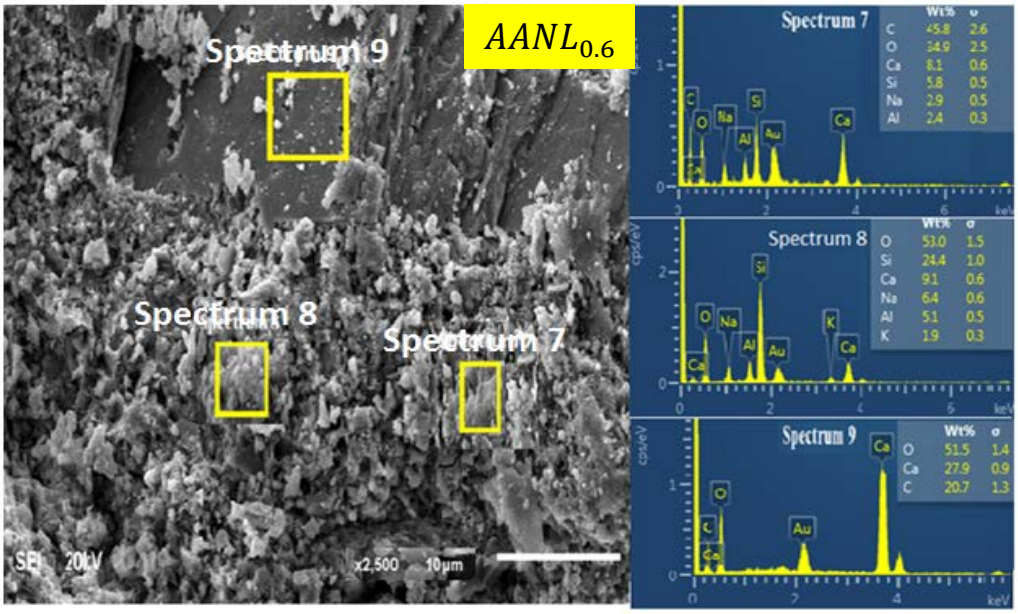

Figure 12. SEM/EDS of binary blended alkali-activated natural pozzolan and limestone powder ($AANL_{0.6}$).

3.5. Effect of NP on microstructures and bonds of alkali-activated mortar

The XRF results in Table 2 show that NP contains SiO_2 (74 %), Al_2O_3 (13 %), K_2O(5 %), Na_2O (4 %) and CaO (2 %), which can also be expressed as $C(N_2)A_7S_{37}$ and $K_3A_7S_{37}$. The XRD results in Figure 3 also confirmed the presence of the amorphous phase of NP as indicated by the diffusive halo diffraction peaks between 15° and 40°. The peaks in the NP diffractogram include the plagioclase (albite/Anorthite (Ca, Na)$Al_2Si_2O_8$), microcline ($KAl_2Si_3O_8$) and quartz (SiO_2). Alkali activation of NP structures resulted in the dissolution of the $C(N_2)A_7S_{37}$ and $K_3A_7S_{37}$ bonds and the formation of potassium-aluminosilicate hydrate (KASH), sodium-aluminosilicate hydrate (NASH) and calcium-aluminosilicate hydrate (CASH). The SiO_2 from Na_2SiO_3(aq) supplies the soluble Si ions while $NaOH_{(aq)}$ provides the OH^- for bond cleaving. Al and Si in NP became pentavalent as a result of OH^- attachment, hence severing the Si-O-Si, Al-O-Al, or Al-O-Si bond.

The 5- and 6- coordinated Al in complex form is converted to 4-coordination upon dissolution, The Al-O-Al being the weakest bond ruptured first to form Al-O that reacts with SiO_2 from $Na_2SiO_{3(aq)}$ to form aluminosilicate oligomer. The Al-O- (negative) is charged balanced by the positive charged (K, Ca or Na). The next stage is the agglomeration of these monomers -Al-O-KOH, -Al-O-NaOH, and -Al-O-CaOH together with -Si-O-Si to form KASH, NASH and CASH, respectively. The XRD results in Figure 8a also revealed the formation albite ($Na_{0.98}Ca_{0.02}Al_{1.02}Si_3O_8$) similar to (C, NASH), Leucite ($KAlSi_2O_6$) similar in form to KASH with quartz.

A very low 28-day compressive strength of 8.9 MPa was obtained in $AANL_0$, this is attributed to the formation portlandite ($Ca(OH)_2$) as a result of the presence OH^- vibration of a broad peak centered at wavenumber 3462 cm^{-1} (FTIR in Figure 9d) which is absent in the raw NP as shown in Figure 9b. In addition, FTIR in Figure 9d shows that there is an asymmetric stretching of H-O-H formed due to hydrogen bonding at a wavenumber of 2331 cm^{-1} coupled with bending of an unbound water molecule at 1645 cm^{-1} and this could constitute to weak microstructure. Furthermore, Figure 10 shows the SEM image and the EDS result of $AANL_0$, $AANL_0$ SEM image appeared to be non-homogenous, flaky and non-dense structure due to the presence of air voids. This is responsible for the low compressive strength recorded in $AANL_0$. The EDS results also show high Si/Al (4.5~7) and low Ca/Si (0.04) (spectrum 3). The low Ca/Si could also have contributed to the negative strength development in the $AANL_0$.

3.6. Effect of NP/LSPW on reaction product, bond characteristic and microstructures of alkali-activation AANL mortar

The alkali activation of the combined precursors (NP/LSPW) gives the maximum 28-day compressive strength of 27 MPa with 60 % LSPW combination with 40 % NP ($ANNL_{0.6}$). The reaction products are calcite ($CaCO_3$), quartz ((SiO_2), albite ($NaAlSi_3O_8$), anorthite ($CaAl_2Si_2O_8$), gehlenite ($Ca0.Al_2O_3SiO_2$) as revealed in the XRD in Figure 8c. Anorthite ($CaAl_2Si_2O_8$) and gehlenite ($Ca0.Al_2O_3SiO_2$) are present in $ANNL_{0.6}$ but absent in $ANNL_0$ and $ANNL_1$ as depicted in Figure. 8. These two compounds contributed positively to the compressive strength development of $ANNL_{0.6}$. Furthermore, Figure 12 shows the SEM image and the EDS result of $ANNL_{0.6}$, $ANNL_{0.6}$ SEM image appeared to be homogenous and dense in the microstructure. There are two distinct regions on the image. Spectrum 7 showing a dense microstructure is the reactive products while spectrum 9 shows the reactive $CaCO_3$. The calcite has pores filling effect on the microstructure, which also favours the compressive strength development. The EDS of $ANNL_{0.6}$ also, show the lowest Si/Al (2.4~4.9) in comparison with $ANNL_1$

(Si/Al (4~7) and $ANNL_0$ (Si/Al) (4.5~7). When the Ca/Si is 1.4 (spectrum 7), this value is 34 % greater than Ca/Si in $ANNL_0$. The Ca/Si was higher in $ANNL_{0.6}$ due to soluble Ca^{2+} contribution from LSPW. The Ca^{2+} contributes to the strength development by both pores filling and bonding with O-Si-O and O-Al-O and the OH^{-1} to form CaOH-Si-O-AlCaOH.

FTIR spectrum in Figure 9e validate the presence of hydroxylation of a widespread peak vibration centered at wavenumber 3464 cm^{-1} in $ANNL_{0.6}$ which is weaker if compared to that of $ANNL_0$ and $ANNL_1$ (Figure 8c/8d). Besides, there is asymmetric stretching of H-O-H formed due to hydrogen bonding at a wavenumber of 2357 cm^{-1} coupled with bending of a very little water molecule at 1645 cm^{-1} if compared to that of $ANNL_0$ and $ANNL_1$. The lesser the water present in the micropores, the higher the strength.

4. Conclusions

In this research, the alkali-activated mortar was synthesized by utilizing limestone powder waste (LSPW) from the tiles manufacturing industry and natural pozzolan (NP) from a volcanic source. The effects of LSPW and NP on the workability, setting time, reaction products, strengths development, bond characteristics and the microstructural properties of the developed alkali-activated binary blending of LSPW and NP (AALN) mortar were investigated and the following are the summary of the conclusions:

1. The dearth in CaO in NP decreases the consistency of the mixtures while the more the quantity of LSPW of higher calcium source, the more the flowability of the mixture. However, setting time reduces with the higher content of LSPW due to early integration and formation of calcium silicate hydrate.

2. There was an insignificant strength development when the LSPW and NP were used independently (6–9 MPa) due to the formation of unstable aluminosilicate framework and portlandite in the former and the latter systems due to the absence of SiO_2 and CaO, respectively.

3. The optimum percentage of NP in the binary blending is 40 % while LSPW constituted 60 % in the mixture that resulted in the 28-day maximum compressive strength of 27 MPa.

4. Formation of anorthite ($CaAl_2Si_2O_8$) and gehlenite ($Ca0.Al_2O_3SiO_2$) in the synergy of the alkali-activated NP and LSPW contributed positively to the strength development.

5. The pore-filling effect caused by the presence of calcite in the product resulted from the binary combination of NP and LSPW.

6. The rough texture of the micrograph of alkali-activated NP was characterized with high porosity turned to promote denser and smooth microstructure in the presence of LSPW.

5. Acknowledgements

The authors gratefully acknowledge the support from the Research Management Centre (RMC) Universiti Teknologi Malaysia (UTM), Grant no: 16H94. The center for Engineering Research (CER), Research Institute, King Fahd University of Petroleum and Minerals, Dhahran, Saudi Arabia and the University of Hafr Al-Batin, Hafr Al-Batin, Saudi Arabia.

References

1. Scrivener, K.L., John, V.M., Gartner, E.M. Eco-efficient cements: Potential, economically viable solutions for a low-CO_2, cementbased materials industry [Online]. 2015. URL: https://www.devalt.org/Pdf/L2_SixThemePdfs/2016-UNEPReport-Complete4 (1).pdf
2. CEMBUREAU Activity Report 2015. 2015. URL: https://cembureau.eu/media/1503/2015activityreport_cembureau.pdf
3. Damtoft, J.S., Lukasik, J., Herfort, D., Sorrentino, D., Gartner, E.M. Sustainable development and climate change initiatives. 2008. 38. Pp. 115–127. DOI: 10.1016/j.cemconres.2007.09.008
4. Andrew, R.M. Global CO 2 emissions from cement production. 2017. (August). Pp. 1–52.
5. Provis, J.L., van Deventer, J.S.J. Alkali avtivated materials. 2014. DOI: 10.1007/978-94-007-7672-2
6. Luukkonen, T., Abdollahnejad, Z., Yliniemi, J., Kinnunen, P., Illikainen, M. One-part alkali-activated materials. Cement and Concrete Research. 2018. 103 (October). Pp. 21–34. DOI: 10.1016/j.cemconres.2017.10.001
7. Najimi, M., Ghafoori, N., Sharbaf, M. Alkali-activated natural pozzolan/slag mortars: A parametric study. Construction and Building Materials. 2018. 164. Pp. 625–643. DOI: 10.1016/j.conbuildmat.2017.12.222
8. Najimi, M., Sobhani, J., Ahmadi, B., Shekarchi, M. An experimental study on durability properties of concrete containing zeolite as a highly reactive natural pozzolan. Construction and Building Materials. 2012. 35. Pp. 1023–1033. DOI: 10.1016/j.conbuildmat.2012.04.038
9. Ibrahim, M., Megat Johari, M.A., Maslehuddin, M., Rahman, M.K., Salami, B.A., Mohamed, H.D. Influence of composition and concentration of alkaline activator on the properties of natural-pozzolan based green concrete. Construction and Building Materials. 2019. 201. Pp. 186–195. DOI: 10.1016/j.conbuildmat.2018.12.117
10. Karim, M.R., Zain, M.F.M., Jamil, M., Lai, F.C. Fabrication of a non-cement binder using slag, palm oil fuel ash and rice husk ash with sodium hydroxide. Construction and Building Materials. 2013. 49. Pp. 894–902. DOI: 10.1016/j.conbuildmat.2013.08.077
11. Salami, B.A., Megat Johari, M.A., Ahmad, Z.A., Maslehuddin, M. Impact of added water and superplasticizer on early compressive strength of selected mixtures of palm oil fuel ash-based engineered geopolymer composites. Construction and Building Materials. 2016. 109. Pp. 198–206. DOI: 10.1016/j.conbuildmat.2016.01.033

12. Kubba, Z., Fahim Huseien, G., Sam, A.R.M., Shah, K.W., Asaad, M.A., Ismail, M., Tahir, M.M., Mirza, J. Impact of curing temperatures and alkaline activators on compressive strength and porosity of ternary blended geopolymer mortars. Case Studies in Construction Materials. 2018. 9. Pp. e00205. DOI: 10.1016/j.cscm.2018.e00205
13. Salami, B.A., Megat Johari, M.A., Ahmad, Z.A., Maslehuddin, M., Adewumi, A.A. Impact of Al(OH)3addition to POFA on the compressive strength of POFA alkali-activated mortar. Construction and Building Materials. 2018. 190. Pp. 65–82. DOI: 10.1016/j.conbuildmat.2018.09.076
14. Yusuf, M.O. Performance of slag blended alkaline activated palm oil fuel ash mortar in sulfate environments. Construction and Building Materials. 2015. 98. Pp. 417–424. DOI: 10.1016/j.conbuildmat.2015.07.012
15. Najamuddin, S.K., Megat Johari, M.A., Maslehuddin, M., Yusuf, M.O. Synthesis of low temperature cured alkaline activated silicomanganese fume mortar. Construction and Building Materials. 2019. 200. Pp. 387–397. DOI: 10.1016/j.conbuildmat.2018.12.056
16. Deb, P.S., Nath, P., Sarker, P.K. The effects of ground granulated blast-furnace slag blending with fly ash and activator content on the workability and strength properties of geopolymer concrete cured at ambient temperature. Materials and Design. 2014. 62. Pp. 32–39. DOI: 10.1016/j.matdes.2014.05.001
17. Criado, M., Aperador, W., Sobrados, I. Microstructural and Mechanical Properties of Alkali Activated Colombian Raw Materials. Materials. 2016. 9 (3). Pp. 158. DOI: 10.3390/ma9030158
18. Lee, N.K., Lee, H.K. Setting and mechanical properties of alkali-activated fly ash/slag concrete manufactured at room temperature. Construction and Building Materials. 2013. 47. Pp. 1201–1209. DOI: 10.1016/j.conbuildmat.2013.05.107
19. Sinthaworn, S., Nimityongskul, P. Effects of temperature and alkaline solution on electrical conductivity measurements of pozzolanic activity. Cement and Concrete Composites. 2011. 33 (5). Pp. 622–627. DOI: 10.1016/j.cemconcomp.2011.02.012
20. Topçu, I.B., Toprak, M.U., Uygunoğlu, T. Durability and microstructure characteristics of alkali activated coal bottom ash geopolymer cement. Journal of Cleaner Production. 2014. 81. Pp. 211–217. DOI: 10.1016/j.jclepro.2014.06.037
21. Adesanya, E., Ohenoja, K., Luukkonen, T., Kinnunen, P., Illikainen, M. One-part geopolymer cement from slag and pretreated paper sludge. Journal of Cleaner Production. 2018. 185. Pp. 168–175. DOI: 10.1016/j.jclepro.2018.03.007
22. Erdoğan, S.T. Inexpensive intumescent alkali-activated natural pozzolan pastes. Journal of the European Ceramic Society. 2015. 35 (9). Pp. 2663–2670. DOI: 10.1016/j.jeurceramsoc.2015.03.017
23. Moufti, M.R., Sabtan, A.A., El-Mahdy, O.R., Shehata, W.M. Assessment of the industrial utilization of scoria materials in central Harrat Rahat, Saudi Arabia. Engineering Geology. 2000. 57 (3–4). Pp. 155–162. DOI: 10.1016/S0013-7952(00)00024-7
24. goleman, daniel; boyatzis, Richard; Mckee, A. Perlite Statistics and Information. Journal of Chemical Information and Modeling. 2019. 53 (9). Pp. 1689–1699. DOI: 10.1017/CBO9781107415324.004
25. Silva, G., Castañeda, D., Kim, S., Castañeda, A., Bertolotti, B., Ortega-San-Martin, L., Aguilar, R. Analysis of the production conditions of geopolymer matrices from natural pozzolan and recycled construction and demolition wastes. Submitted to Construction and Building Materials. 2019. 215. Pp. 633–643. DOI: 10.1016/j.conbuildmat.2019.04.247
26. Mageed, A.A., AbdelHaffez, S. Utilization of Limestone Dust in Brick Making. Journal of Engineering Sciences. 2012. 40 (3). Pp. 913–922.
27. Turgut, P. Limestone dust and glass powder wastes as new brick material. Materials and Structures/Materiaux et Constructions. 2008. 41 (5). Pp. 805–813. DOI: 10.1617/s11527-007-9284-3
28. Antoni, M., Rossen, J., Martirena, F., Scrivener, K. Cement substitution by a combination of metakaolin and limestone. Cement and Concrete Research. 2012. 42 (12). Pp. 1579–1589. DOI: 10.1016/j.cemconres.2012.09.006
29. Ghafoori, N., Najimi, M., Radke, B. Natural Pozzolan-based geopolymers for sustainable construction. Environmental Earth Sciences. 2016. 75 (14). Pp. 1–16. DOI: 10.1007/s12665-016-5898-5
30. Ibrahim, M., Azmi, M., Johari, M., Kalimur, M., Maslehuddin, M. Effect of alkaline activators and binder content on the properties of natural pozzolan-based alkali activated concrete. Construction and Building Materials. 2017. 147. Pp. 648–660. DOI: 10.1016/j.conbuildmat.2017.04.163
31. Cwirzen, A., Provis, J.L., Penttala, V., Habermehl-Cwirzen, K. The effect of limestone on sodium hydroxide-activated metakaolin-based geopolymers. Construction and Building Materials. 2014. 66. Pp. 53–62. DOI: 10.1016/j.conbuildmat.2014.05.022
32. Yuan, B., Yu, Q.L., Brouwers, H.J.H. Assessing the chemical involvement of limestone powder in sodium carbonate activated slag. Materials and Structures/Materiaux et Constructions. 2017. 50 (2). DOI: 10.1617/s11527-017-1003-0
33. ASTM Standard C191 Standard Test Methods for Time of Setting of Hydraulic Cement by Vicat Needle; ASTM C191-08. American Society for Testing and Materials. (C). 2008. Pp. 1–8. DOI: 10.1520/C0191-08.2
34. ASTM Standard Test Method for Flow of Hydraulic Cement Mortar. Astm C1437-15. 2015. Pp. 1–2. DOI: 10.1520/C1437-15.2
35. American Society of Testing Materials Standard Specification for Portland Cement. ASTM International. June 1999. Pp. 1–6. DOI: 10.1520/C0010
36. Quercia, G., Hüsken, G., Brouwers, H.J.H. Water demand of amorphous nano silica and its impact on the workability of cement paste. Cement and Concrete Research. 2012. 42 (2). Pp. 344–357. DOI: 10.1016/j.cemconres.2011.10.008
37. Duxson, P., Provis, J.L. Designing precursors for geopolymer cements. Journal of the American Ceramic Society. 2008. 91 (12). Pp. 3864–3869. DOI: 10.1111/j.1551-2916.2008.02787.x
38. Yusuf, M.O., Megat Johari, M.A., Ahmad, Z.A., Maslehuddin, M. Strength and microstructure of alkali-activated binary blended binder containing palm oil fuel ash and ground blast-furnace slag. Construction and Building Materials. 2014. 52. Pp. 504–510. DOI: 10.1016/j.conbuildmat.2013.11.012

Contacts:

Adeshina Adewumi, +601114240744; adewumi@graduate.utm.my
Mohammad Ismail, +6075531503; mohammad@utm.my
Mohd Azreen Mohd Ariffin, +60163352841; mohdazreen@utm.my
Moruf Yusuf, +966552545213; moruf@uhb.edu.sa
Mohammad Maslehuddin, +966500026404; muddin@kfupm.edu.sa
Hatim Mohamed, +96656950361; dmhatim@kfupm.edu.sa